3.3. The BEaTriX full simulation code

Besides the simulation of the mirror alone, it is important to understand whether the finishing of the mirror surface is sufficient to guarantee the collimation, uniformity, and intensity properties of the expanded beam. We have thereby used the full BEaTriX simulation program (Figure 8), already developed and used to define the fabrication and the alignment tolerances of the entire system.[19] The following input data have been used:

- A source radiance of 10^{11} ph/s/sterad (in the Kα doublet) from a Ti-anode source of 35 μm FWHM;
- X-ray absorption in the residual atmosphere (10^{-6} mbar);
- reflectivity of the Pt-coated paraboloidal mirror at 0.9 deg incidence;
- paraboloidal mirror metrology (shape error + 2D scattering);
- reflectivity of a Si (220) double CCC, with a relative 12 arcsec rotation in order to narrow the energy passing band to 0.05 eV;[15]
- reflectivity and dispersivity of a Si (220) crystal cut at an asymmetry angle of 44.592 deg;
- all the possible misalignments between components.

We so obtain as output the expected vertical and horizontal divergence, dimensions, intensity, and uniformity of the expanded beam. Optionally, one can also simulate an SPO MM module that focuses the expanded beam.

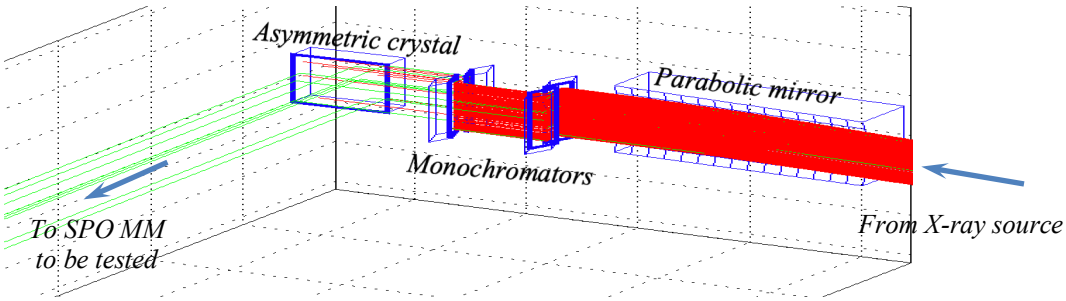

Figure 8: a simple graphical rendition of the BEaTriX simulation code. The rays from the X-ray source are pre-selected by a slit properly shaped to filter only the rays that will finally strike upon the asymmetric crystal. Red rays are absorbed by some optical element. Eventually, green rays populate the expanded beam.

In order to get statistically significant results, 10^7 rays need to be launched at least. This means that, to keep the computation time within reasonable limits, rays cannot be traced at small steps as usual. Rays are traced from their origin in the source to the intersection with each optical element, in a single "big leap", computing the intersection point analytically. This is very easy in the case of crystals, because their surfaces are planar. Given the position of a ray $\underline{r}_0$ and its direction $\underline{k}_0$ before reflection (where $|\underline{k}_0| = 1$), the ray is represented by the equation:

$$\vec{r}_1(t) = \vec{r}_0 + t\vec{k}_0 \tag{2}$$

where t is a positive parameter expressing the distance of $\underline{r}_1$ from $\underline{r}_0$. The equation of a reflecting planar face π with normal $\underline{n}_\pi$, independent of the impact point, and passing by a point $\underline{r}_c$ (e.g., the face center) is

$$(\vec{r}_1 - \vec{r}_c) \cdot \vec{n}_\pi = 0. \tag{3}$$

By substitution, one immediately obtains the value of t where intersection occurs:

$$t = \frac{(\vec{r}_c - \vec{r}_0) \cdot \vec{n}_\pi}{\vec{k}_0 \cdot \vec{n}_\pi} \tag{4}$$

and from Eq. 2, the coordinates of the reflection point. The incidence angle α_π is derived from $\sin\alpha_\pi = \underline{k}_0 \cdot \underline{n}_\pi$ and, for a symmetric reflection, the direction of the reflected ray (Eq. A.2) is $\underline{k}_1 = \underline{k}_0 - 2(\underline{k}_0 \cdot \underline{n}_\pi)\underline{n}_\pi$. The intersection point of the ray with the paraboloidal surface is computed in a similar manner, accounting for the variation of the normal $\underline{n}$ throughout the surface and the mirror imperfections (see Appendix A). For the beam expander, reflection is computed from the normal to the crystalline planes $\underline{n}_{\pi'}$, and accounting for the dispersivity properties of asymmetric crystals:[18]

$$\vec{k}_2 - \vec{k}_1 = \vec{n}_{\pi'} \frac{\lambda}{d_{220}}. \tag{5}$$

4. MIRROR PERFORMANCE SIMULATIONS VS. TESTS AT PANTER

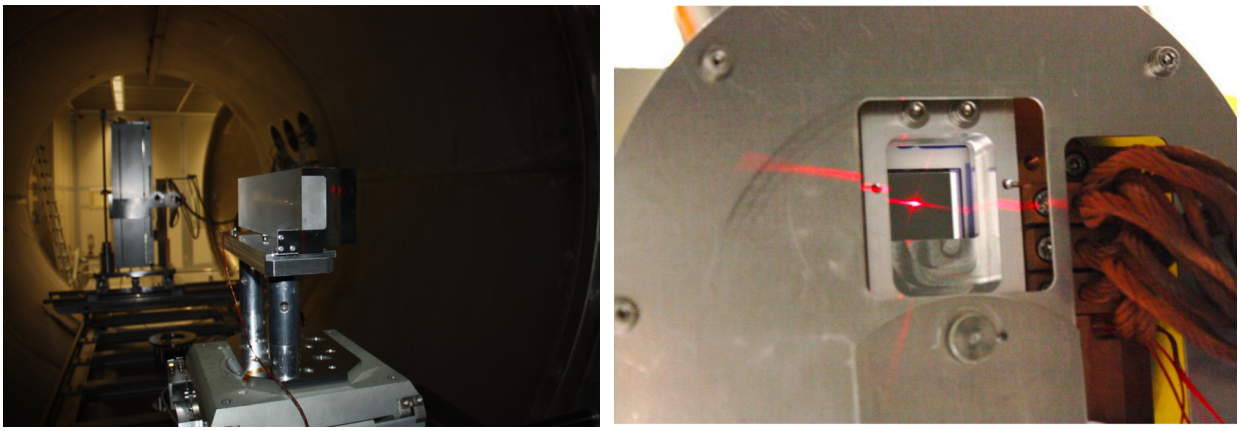

Figure 9: the BEaTriX mirror at PANTER. Left: before coating, in the PANTER vacuum tank. The detector stage, housing the TRoPIC and the PIXI detectors, is visible in the background. Right: the alignment laser, sharply focused on the TRoPIC sensor.

A fundamental step in the BEaTriX mirror finishing has been represented by full-illumination X-ray tests at PANTER, pre- and post-coating, aiming at confirming the predictions from metrology and at accepting the mirror for installation in the BEaTriX facility. The mirror was mounted in the PANTER vacuum tank and pre-aligned with the laser beam (Figure 9). In a first stage, the mirror has been probed with the low-diverging beam propagating freely from the PANTER source (127 m away). Due to the very good optical quality of the mirror, the coma aberration due to the source finite distance is the dominant term (Figure 6), contributing to the total HEW with 4.5 arcsec.

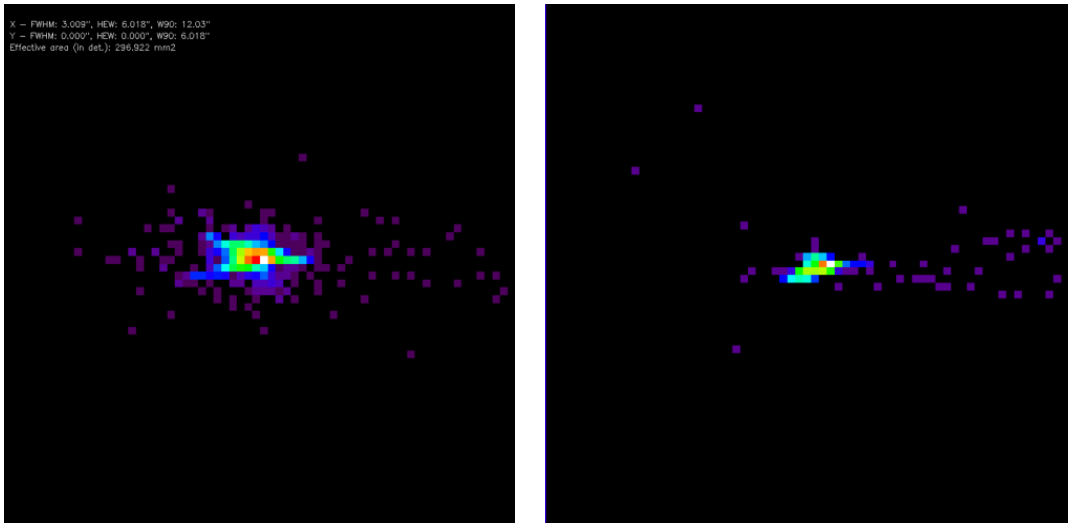

Figure 10: the best focus of the uncoated BEaTriX mirror at 1.49 keV with TRoPIC spatial resolution (pixel size: 3.3 arcsec) and in diverging *beam setup. Left: from simulation, HEW = 5 arcsec. Right: measured with TRoPIC, HEW = 4.8 arcsec. A 4.5 arcsec contribution comes from the divergence of the incoming beam.*

Nevertheless, the focus appeared very sharp and comparable in size with the detector pixels (TRoPIC: 75 μm, PIXI: 20 μm). The tests performed with the diverging beam at 1.49 keV revealed excellent agreement between predictions and experimental results (Figure 10). The HEW measurement in the best focus - which is, in diverging setup, shifted 200 mm downstream - returned 4.8 ± 1.6 arcsec at 1.49 keV and an absolute focal length of 4956 mm from the mirror center, as per our expectations.

As mentioned in Sect. 3.2, the 1.49 keV X-ray beam at PANTER can be made parallel using a zone plate.[26] The parallel beam setup removed completely the coma aberration from the setup and so yielded even better results (Figure 11, center). Even with some uncertainty due to the background noise in the PIXI camera and the finite pixel size (0.9 arcsec), **the measured *HEW is close to 3 arcsec*** and perfectly aligned to the simulation (Figure 11, left). The measured

value also includes the contribution of the source size at PANTER (approx. 0.5 arcsec), so the intrinsic HEW of the mirror itself is probably smaller.

The mirror performances did not relevantly vary from before to after coating deposition at DTU in between the two campaigns at PANTER (Figure 11, right). After the PANTER tests, the coated surface was also re-measured with the CCI, and no roughness increase was observed following the coating process, witnessing the excellent quality of the Pt+Cr reflective layer. After coating, the mirror has become reflective at 4.51 keV, an energy where the zone plate does not work; hence, we have no direct measurement in parallel beam at the X-ray energy of operation. Measurements performed with the diverging beam at this energy, however, returned a HEW near 6.5 arcsec. The 1.5 arcsec increase is probably due to the contribution of mirror areas *outside* the region that will reflect toward the asymmetric crystal and that are known to have a much worse roughness. Moreover, those areas would not contaminate the expanded beam, because a mirror slit will prevent them from being illuminated by the microfocus source.

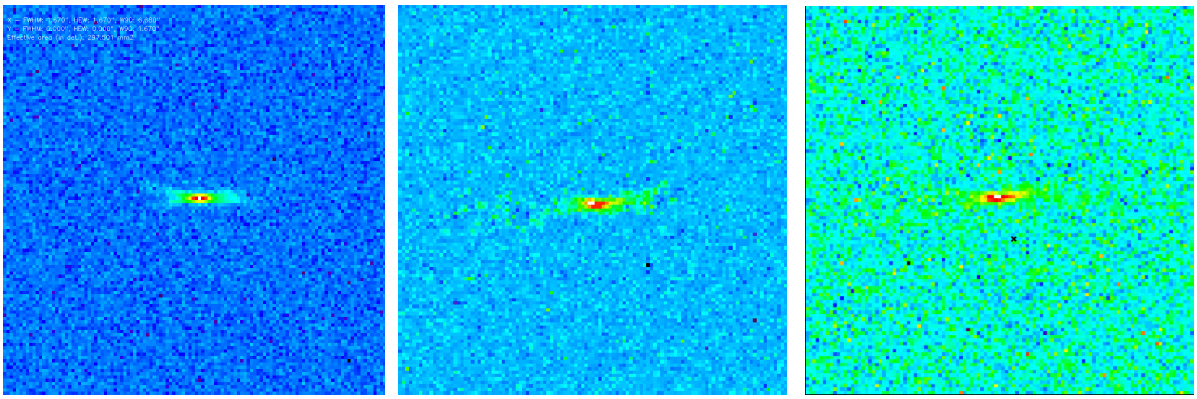

Figure 11: the best focus of the BEaTriX mirror at 1.49 keV with PIXI spatial resolution (pixel size: 0.9 arcsec) and in parallel *beam setup. Left: from simulation, HEW = 2.7 arcsec. Center: uncoated mirror, measured with PIXI, HEW = 3.1 arcsec. Right: after coating, measured with PIXI, HEW = 2.8 arcsec.*

5. SIMULATIONS OF THE EXPANDED BEAM COLLIMATION AND UNIFORMITY

5.1. The ideal BEaTriX system

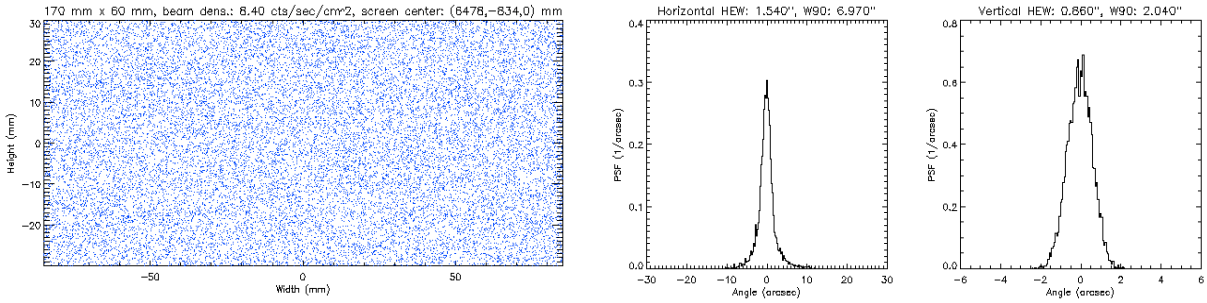

Figure 12: full simulation of the BEaTriX expanded beam for a perfect paraboloidal mirror and perfect alignment. Left: beam uniformity and dimensions. Right: due to the source size and the spectral bandpass through the monochromator, an ideal optical chain returns a beam with a HEW = 0.9 arcsec in vertical and 1.5 arcsec in horizontal.

Running the full BEaTriX simulation program (Figure 8) with a flawless paraboloidal mirror and all the components perfectly aligned, the result is shown in Figure 12. The viewgraphs correspond to the best achievable results in the BEaTriX facility: a 17 cm × 6 cm uniform beam, with a flux density of 8.4 counts/s/cm^2. The vertical divergence, almost solely due to the dimensions of the microfocus X-ray source, is near 0.9 arcsec HEW and will represent the divergence in the incidence plane of the MMs to be tested, therefore it is the most important parameter for probing their focusing properties. The horizontal divergence (HEW = 1.5 arcsec) is determined by the source size *and* by the spectral bandpass out of the monochromators.[19] This divergence component is the most sensitive to mirror imperfections, because a poor collimation by the paraboloid would increment the angle-energy combinations fulfilling the Bragg law in the symmetric crystals. This would in turn increase the angular dispersion in the asymmetric crystal.

5.2. Accounting for mirror imperfections and metrology

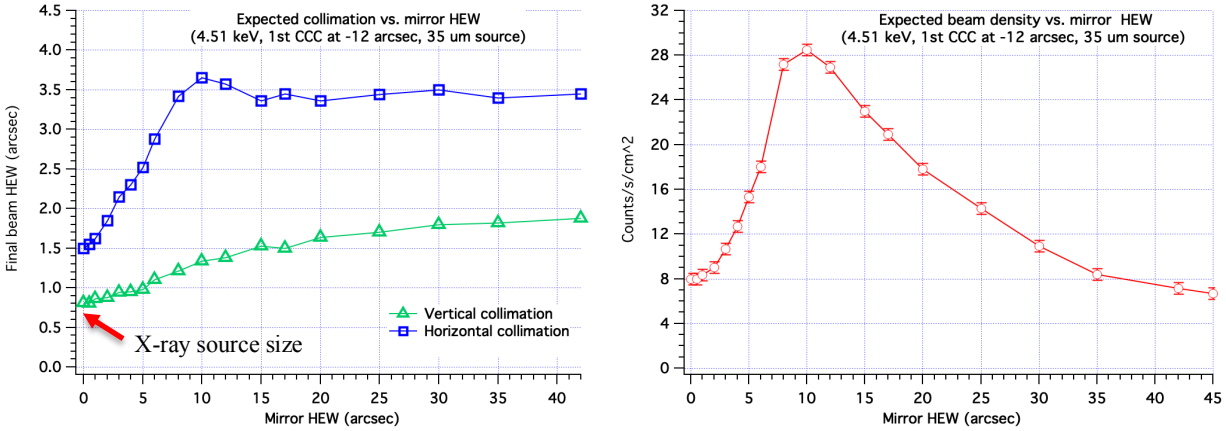

Figure 13: simulated impact of imperfections of the BEaTriX collimating mirror on (left) the vertical and horizontal collimation and (right) the beam flux. The vertical collimation is mostly affected by the size of the X-ray source, while the horizontal collimation is more severely degraded as the mirror quality gets worse. The beam intensity exhibits a peak where the mirror HEW starts to exceed the monochromators' rocking curve widths. However, the price for higher intensity can be a nonuniform beam.

Performing an extensive set of simulations with the BEaTriX simulation code and modeling variable levels of optical finishing,[19] this time up to a 45 arcsec HEW for the mirror (which was not far, indeed, from the initial quality of the pre-formed mirror),[15] we obtain the trends in Figure 13. The vertical collimation, essentially depending on the source size, is the least sensitive to the mirror quality. In contrast, the horizontal divergence degrades in proportion to the mirror quality, up to a plateau from 10 arcsec onwards. The saturation is explained by the rejection of rays impinging on the symmetric crystals with angles out of the narrow rocking curves of Si (220) diffraction order. At these angles, indeed, the energy shift needed to fulfill the Bragg condition would be larger than the natural width of the Ti-Kα1 line. This also justifies the intensity drop beyond 10 arcsec (Figure 13, right). The current situation of BEaTriX with a paraboloidal mirror having a measured HEW in the 3 - 4.5 arcsec range locates *the vertical divergence at 1 arcsec HEW and the horizontal one at 2.2 arcsec HEW*, perfectly suitable for testing SPO MMs. We also note that, thanks to the filtering effect of monochromators, a degradation by *1 arcsec* in the paraboloidal mirror will result in just a *0.2 arcsec* worsening of the expanded beam.

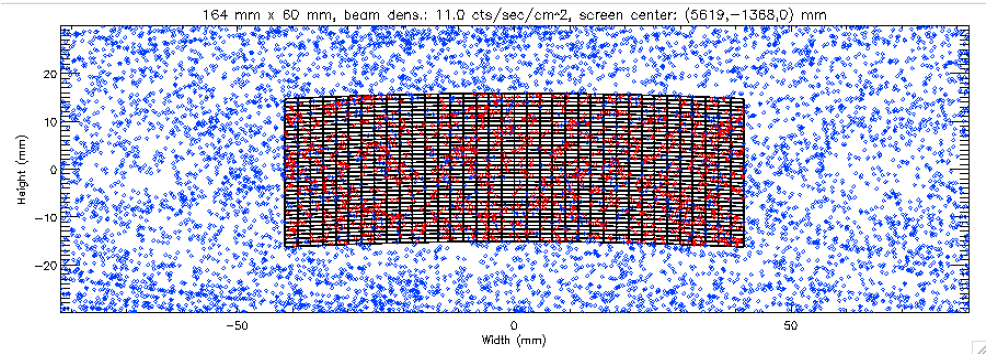

Figure 14: expanded beam dimensions and uniformity expected from the current status of the collimating mirror in BEaTriX. Also simulated is the incidence on a single XOU of ATHENA (one of the row No.8 in the current ATHENA design). Red markers represent the rays that have struck on a reflective surface of the SPO mirror module.

It is also possible to directly forecast the properties of the expanded beam from the current paraboloid metrology dataset (Sect. 3.1). The result is shown in Figure 14, where we have simulated the insertion of a mirror module in the expanded beam, and in Figure 15. The collimation and the intensity of the expanded beam match very well the values obtained from the expectation trend shown in Figure 13. Even if the beam uniformity is somehow altered by the mirror imperfections, the nonuniformity will not compromise the optical module PSF measurement. Neither will it hamper the effective area measurement, if the focused intensity is properly normalized to the beam intensity that will actually enter the mirror aperture (Sect. 5.3).

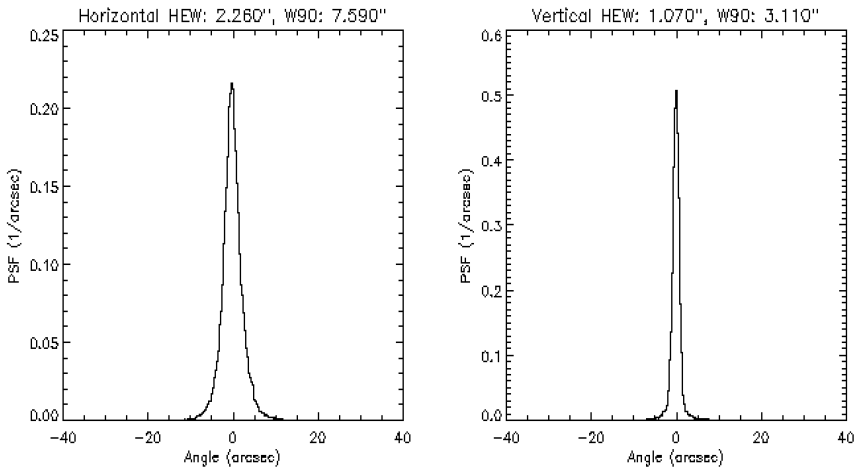

Figure 15: expected collimation in the expanded beam of BEaTriX, from the final status of the paraboloidal mirror.

5.3. Simulating the incidence on an SPO mirror module

An alternative method to assess the properties of the BEaTriX beam consists in prolonging the ray-tracing to the mirror module chamber (Figure 3) and simulating the reflection process in the complex structure of a silicon pore optic, as already sketched in Figure 14. For simplicity, but without loss of significance, we have taken an X-ray Optical Unit (XOU, half a MM) of the row No. 8 in the current mirror module assembly in the ATHENA design, assumed perfect (HEW = 0 arcsec) and 100% reflective. If the mirror module is exactly aligned on-axis, rays in the expanded beam can either be stopped on a membrane/rib wall, or be reflected. A small fraction of the reflected rays misses the second reflection and is baffled by the SPO structures, while all the others make the second reflection and reach the focus.

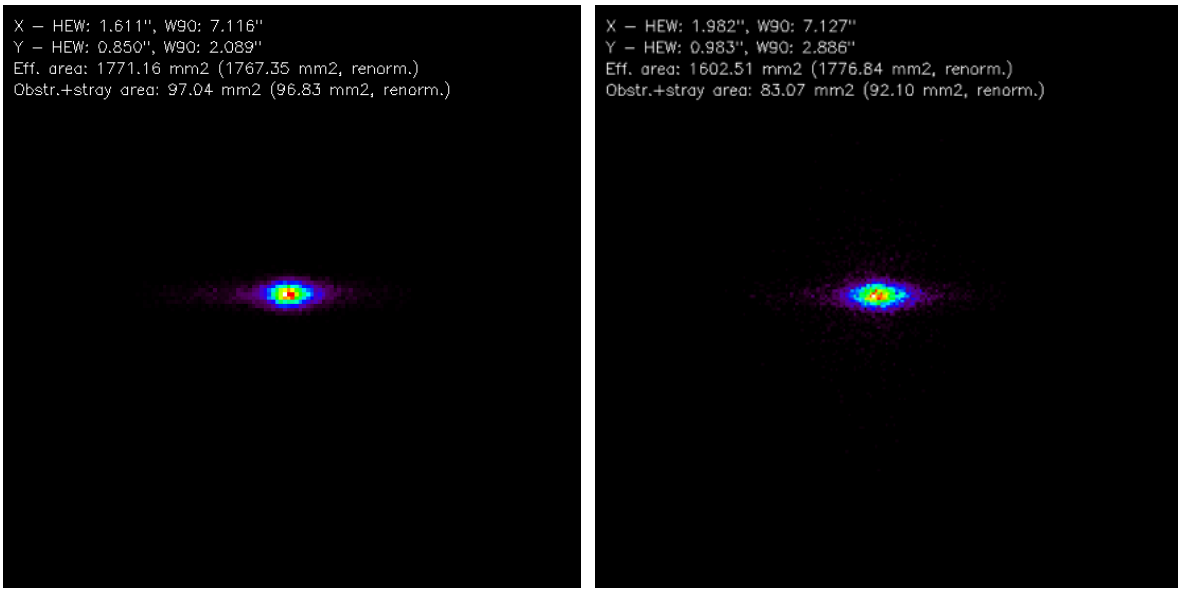

Figure 16: simulated focus of a perfect mirror module in the BEaTriX expanded beam. Left: in a perfect BEaTriX system. Right: with the current manufacturing status of the paraboloidal mirror. In both cases, the focus appears elongated horizontally due to the better beam collimation in the vertical plane, which is also the incidence plane of the MM to be tested. Residual mirror imperfections chiefly degrade the focus horizontally. The images have a 3 mm size.

Figure 16 shows what to expect in the focus of the MM, at the end of the long arm of BEaTriX. In an ideal system (Sect. 5.1), the focus has the shape of an ellipse with the axes equal to the vertical and horizontal HEW values reported in Figure 12. With the real paraboloid, the vertical size will be only slightly larger, while the horizontal size will be broader due to the increased divergence. In this case also, the focal spot dimensions correspond to the divergence values assessed from the angular deviations (Figure 15).

As for the effective area, the 17.67 cm^2 found with the "perfect" BEaTriX beam is exactly what one would find analytically.[24] Even though nonuniformities in the "real" expanded beam can alter this measurement, renormalizing the focus brightness to the intensity impinging onto the mirror module aperture will allow us retrieving the correct effective area value to within a few percent accuracy (17.76 cm^2).

6. DETECTING SOURCE MISALIGNMENTS VIA WAVEFRONT SENSING

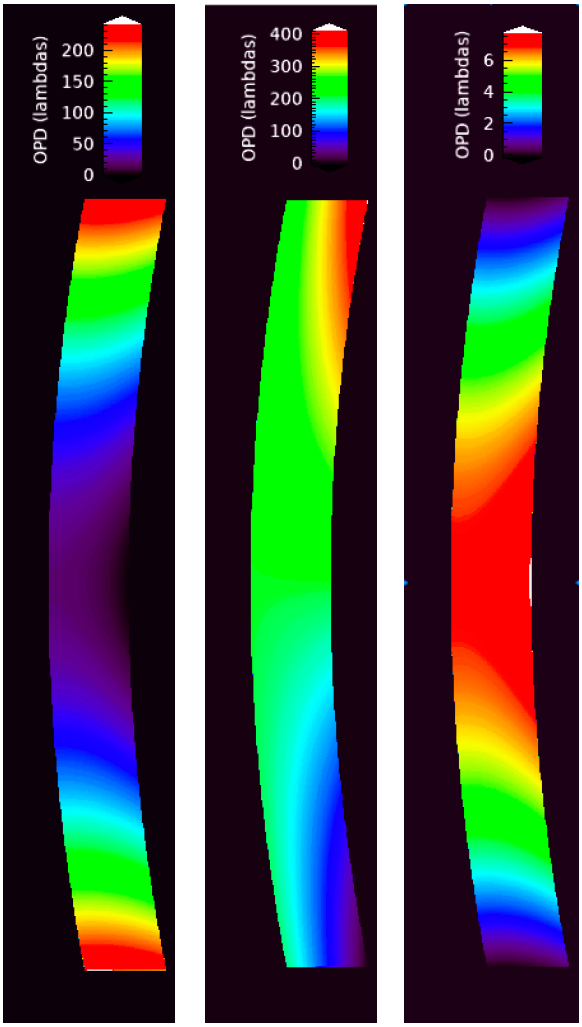

Figure 17: simulated wavefront out of the BEaTriX mirror due to misalignments by 1 mm (left) along the radius; (center) in vertical direction; (right) along the rays. The color scales express the optical path difference in units of lambda.

Just like manufacturing the paraboloidal mirror is a fundamental step, a precise alignment of the mirror focus to the source is also necessary for ensuring the expanded beam collimation. We have already discussed this problem in a previous contribution[19] and determined that accurate alignment in X-rays can be achieved using a wavefront sensor (WFS). Therefore, we are planning to use a WFS in collaboration with Brookhaven National Labs, ENSTA-Paris and Imagine Optic to diagnose the collimated beam out of the BEaTriX mirror. From the wavefront deformation, the mirror-to-source misalignments can be measured and corrected by means of the vacuum motors.

The wavefront deformations expected from the three possible source displacements can be modeled using one of the functionalities implemented in the full BEaTriX simulation program (Sect. 3.3), but the ray statistics requires an unacceptably long time to perform a systematic investigation. We would rather use an approach based on physical optics, reversing the program used to propagate the wavefront to the focus (Figure 6, left). In all the cases considered, the phase shifts used to back-propagate the beam from the source to the detection plane are the projected differences in the radial coordinate between the nominal paraboloid and the paraboloid that would exactly focus the beam at the current location of the source. Three examples, shown in Figure 17, illustrate the expected wavefront shapes that would be detected by the wavefront sensor near the mirror, in the presence of a misaligned source, along three independent directions in space (tilt terms were mostly removed). The wavefront shapes can be analyzed in terms of Zernike polynomials or beamlet displacements out of a Hartmann plate. As already pointed out,[19] source displacements in the incidence plane mainly defocus the beam, while displacements in the sagittal plane twist the wavefront, introducing coma and astigmatism terms. Displacements along the rays exhibit an effect totally similar to the one of displacements along the radius, but the wavefront is much less sensitive to this kind of displacement. A systematic analysis of the wavefront distortion caused by source misalignments will give us confidence with this tool before proceeding to the forthcoming alignment of the paraboloidal mirror in BEaTriX.

7. FINAL REMARKS

The ongoing assembly of the BEaTriX X-ray facility at INAF-Brera and the alignment of the optical components is being assisted by a set of optical simulations. To this aim, we have explored a variety of approaches, based on both geometric and physical optics. Some simulations were addressed at predicting the optical quality of the paraboloidal mirror from the available metrology data, in very good agreement with experiments at PANTER. Other software tools

have been used to predict the effect of the collimating mirror on the divergence, the uniformity, and the intensity of the expanded beam at the different stages of the mirror finishing. As we approach the alignment of the mirror in the 4.51 keV beamline of BEaTriX, wavefront distortion simulations are being suited to gain confidence with the precise alignment process. Future work will extend the simulations to the 1.49 keV beamline of BEaTriX.

APPENDIX A. IN- AND OUT-OF-PLANE SCATTERING IN RAY-TRACING

In a mirror surface described by the rotation of the profile $r(z)$ about the z-axis, the unit normal vector at the ray impact point, located by the cylindrical coordinates (φ_0, z_0), is given by

$$\vec{n} = (-\cos\alpha_0 \cos\varphi_0\,, -\cos\alpha_0 \sin\varphi_0\,, \sin\alpha_0) \tag{A.1}$$

where $\alpha_0 = \tan^{-1}(r'(z_0))$ is the incidence angle for an on-axis ray. The usual formula providing the reflected ray direction, $\underline{k}_1$, as a function of the incident direction $\underline{k}_0$ and the local normal vector:

$$\vec{k}_1 = \vec{k}_0 - 2(\vec{k}_0 \cdot \vec{n})\vec{n} \tag{A.2}$$

(where "·" denotes a scalar product of vectors), returns a final ray direction that is correctly normalized to 1,

$$|\vec{k}_1|^2 = (\vec{k}_0 \cdot \vec{k}_0) - 4(\vec{k}_0 \cdot \vec{n})^2 + 4(\vec{k}_0 \cdot \vec{n})^2 |\vec{n}|^2 = |\vec{k}_0|^2 = 1, \tag{A.3}$$

and forming with the initial ray direction an angle α_{01} such that:

$$\vec{k}_1 \cdot \vec{k}_0 = 1 - 2(\vec{k}_0 \cdot \vec{n})(\vec{k}_1 \cdot \vec{n}). \tag{A.4}$$

In specular reflection, the angle between $\underline{k}_1$ and $\underline{n}$ is the same as between $\underline{k}_0$ and $\underline{n}$, i.e., $\underline{k}_0 \cdot \underline{n} = \sin\alpha_0$, so we get

$$\vec{k}_1 \cdot \vec{k}_0 = 1 - 2\,sin^2\,\alpha_0 = cos\;2\alpha_0; \tag{A.5}$$

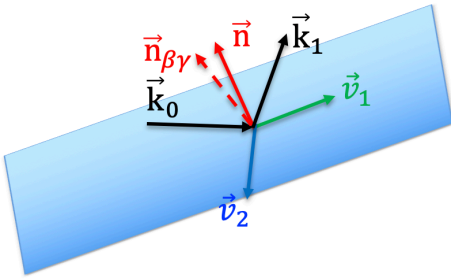

Figure A.1: the reference frame for a proper treatment of in-plane and out-of-plane ray deflections.

which correctly implies that the angle between $\underline{k}_1$ and $\underline{k}_0$ is $\alpha_{01} = 2\alpha_0$. If the mirror is imperfect, in order to preserve the validity of Eq. (A.2), we will have to alter the local normal vector (A.1) to account for both ray deviations: in the incidence plane, and orthogonal to the incidence plane.

As for in-plane scattering, we want $\underline{k}_1$ to form a larger angle with $\underline{k}_0$, i.e., $2\alpha_0+2\beta$. We therefore rotate the normal vector by an angle β in the incidence plane. For the new normal vector $\underline{n}_\beta$ to lie in the ($\underline{k}_0$, $\underline{n}$) plane, it has to be an appropriate linear combination of them. More exactly, we replace $\underline{n}$ in Eq. (A.2) with

$$\vec{n}_\beta = \vec{n}\,cos\,\beta + \vec{v}_1\,sin\,\beta. \tag{A.6}$$

The first term is the component coming from the original normal $\underline{n}$, while the second one, proportional to

$$\vec{v}_1 = \frac{\vec{k}_0 - (\vec{k}_0 \cdot \vec{n})\vec{n}}{\sqrt{1 - (\vec{k}_0 \cdot \vec{n})^2}} \tag{A.7}$$

is the $\underline{k}_0$ component orthogonal to $\underline{n}$ (i.e., $\underline{k}_0$ *minus* its component parallel to $\underline{n}$). We can immediately see that the two components are mutually orthogonal and normalized to 1. The new normal, $\underline{n}_\beta$, is normalized to 1 also:

$$|\vec{n}_\beta|^2 = |\vec{n}|^2 cos^2\,\beta + 2\frac{(\vec{k}_0 \cdot \vec{n}) - (\vec{k}_0 \cdot \vec{n})}{\sqrt{1 - (\vec{k}_0 \cdot \vec{n})^2}} cos\,\beta\,sin\,\beta + |\vec{v}_1|^2\,sin^2\,\beta = \; cos^2\,\beta + sin^2\,\beta = 1, \tag{A.8}$$

and, similarly to Eq. (A.5), the angle between $\underline{k}_0$ and $\underline{k}_1$ takes on the expected value: using Eq. (A.2) with $\underline{n}_\beta$, we get

$$\vec{k}_0 \cdot \vec{k}_1 = 1 - 2\left(\vec{k}_0 \cdot \vec{n}_\beta\right)^2 = 1 - 2\left[\left(\vec{k}_0 \cdot \vec{n}\right)\cos\beta + \left(\vec{k}_0 \cdot \vec{v}_1\right)\sin\beta\right]^2 =$$
$$= 1 - 2[\sin\alpha_0 \cos\beta + \cos\alpha_0 \sin\beta]^2 = 1 - 2\sin^2(\alpha_0 + \beta) = \cos(2\alpha_0 + 2\beta). \quad \text{(A.9)}$$

A deviation in the orthogonal direction by an angle γ, due to out-of-plane scattering, can be modeled adding a third vector component:

$$\vec{v}_2 = \vec{n} \times \vec{v}_1 = \frac{\vec{n} \times \vec{k}_0}{\sqrt{1 - \left(\vec{k}_0 \cdot \vec{n}\right)^2}} \quad \text{(A.10)}$$

("×" means cross vector product), which is also normalized and, clearly, orthogonal to the incidence plane. The perturbed normal vector is therefore represented by an extension of Eq. (A.6) to spherical coordinates:

$$\vec{n}_{\beta\gamma} = \vec{n}\cos\beta\cos\gamma + \vec{v}_1 \sin\beta\cos\gamma + \vec{v}_2 \sin\gamma. \quad \text{(A.11)}$$

Using Eq. (A.11), the reflection direction from the imperfect mirror is obtained generalizing Eq. (A.2):

$$\vec{k}_1 = \vec{k}_0 - 2\left(\vec{k}_0 \cdot \vec{n}_{\beta\gamma}\right)\vec{n}_{\beta\gamma}. \quad \text{(A.12)}$$

We note that, in grazing incidence, the effect of the out-of-plane deflection is automatically damped[23] by a factor of $\tan\alpha_0$. The angle γ can therefore be computed as if the scattering occurred in the tangential plane, just like β, without the need to reduce its amplitude by a factor of $\tan\alpha_0$.

ACKNOWLEDGMENTS

The BEaTriX project is financed by ESA (contract #4000123152/18/NL/BW), AHEAD (grants #654215 and #871158), ASI (grant #2019-27-HH.0) and INAF funds. We thank Philippe Zeitoun (ENSTA-Paris), Ombeline De La Rochefoucauld (Imagine Optic), and Mourad Idir (Brookhaven National Labs) for the interest and the kind collaboration in the project.

REFERENCES

[1]. Bradshaw, M., Burwitz, V., Hartner, G., Langmeier, A., Vacanti, G., et al., "Testing ATHENA optics: a new measurement standard at the PANTER x-ray test facility," Proc. of SPIE 11852, 1185223 (2021)
[2]. Bavdaz, M., Wille, E., Ayre, M., Ferreira, I., Shortt, B., et al., "The Athena x-ray optics development and accommodation," Proc. SPIE 11852, 1185220 (2021)
[3]. Collon, M. J., Babic, L., Barrière, N. M., Bayerle, A., Castiglione, L., et al., "X-ray mirror development and production for the Athena telescope," Proc. SPIE 11852, 118521Z (2021)
[4]. Krumrey, M., Muller, P. et al., "New X-ray parallel beam facility XPBF 2.0 for the characterization of the silicon pore optics," Proc. SPIE 9905, 99055N (2016)
[5]. Vacanti, G., Barrière, N. M., Collon, M.J., Hauser, E., et al., "X-ray testing of Silicon Pore Optics," Proc. SPIE 11119, 1111901 (2019)
[6]. Burwitz, V., Bavdaz, M, Wille, E., Collon, M., et al., "X-ray testing at PANTER of optics for the ATHENA and Arcus Missions," Proc. SPIE 11180, 1118024 (2019)
[7]. Spiga, D., Pareschi, G., Pelliciari, C., et al., "Functional tests of modular elements of segmented optics for x-ray telescopes via an expanded beam facility," Proc. SPIE 8443, 84435F (2012)
[8]. Spiga, D., Pelliciari, C., Bonnini, E., et al., "An expanded x-ray beam facility (BEaTriX) to test the modular elements of the ATHENA optics," Proc. SPIE 9144, 91445I (2014)
[9]. Pelliciari, C., Spiga, D., Bonnini, E., et al., "BEaTriX, expanded soft x-ray beam facility for test of focusing optics, an update," Proc. SPIE 9603, 96031P (2015)
[10]. Spiga, D., Pelliciari, C., Salmaso, B., et al. "Design and advancement status of the Beam Expander Testing X-ray facility (BEaTriX)," Proc. SPIE 9963, 996304 (2016)

[11]. Salmaso, B., Spiga, D., Basso. S., Ghigo, M., Giro, E., Pareschi, G., Tagliaferri, G., Vecchi, G., et al., "Progress in the realization of the beam expander testing x-ray facility (BEaTriX) for testing ATHENA's SPO modules," Proc. SPIE 10699, 1069931 (2018)
[12]. Salmaso, B., Spiga, D., Basso. S., Ghigo, M., Giro, E., Pareschi, G., Tagliaferri, G., Vecchi, et al., "BEaTriX (Beam Expander Testing X-ray facility) for testing ATHENA's SPO modules: advancement status," Proc. SPIE 11180, 1118026 (2019)
[13]. Valsecchi, G., Bianucci, G., Marioni, F., Vernani, D., Zocchi, F., Korhonen, T., Pasanen, M., Pareschi, G., Ferreira, F., Bavdaz, M., Wille, E., Doyle, D., "Facility for alignment, assembly, and integration of the SPO mirror modules onto the ATHENA telescope," Proc. SPIE 11822 (2021)
[14]. Moretti, A., Spiga, D., Sironi, G., Pareschi, G., Basso, S. Tagliaferri, G., Valsecchi, G., Zocchi, F., Vernani, D., Marioni, F., Tordi, M., De Lorenzi, S., Parodi, G., Amisano, F., Corradi, P., Ottolini, M., Ferreira, I., Bavdaz, M., Parissenti, G., La Palombara, N., Uslenghi, M., Civitani, M, Ghigo, M. "The VERT-X calibration facility: development of the most critical parts," Proc. SPIE 11822 (2021)
[15]. Salmaso, B., Basso, S., Cotroneo, V., Ghigo, M., Pareschi, G., Redaelli, E., Sironi, G., Spiga, D., Tagliaferri, G., Vecchi, G., Fiorini, M., Incorvaia, S., Uslenghi, M., Paoletti, L., Ferrari, C., Zappettini, A., Lolli, R., Sanchez del Rio, M., Burwitz, V., Christensen, F., Della Monica Ferreira, D., Gellert, N., Massahi, S., Bavdaz, M., Ferreira, I., "Building the BEaTriX facility for the ATHENA mirror modules X-ray testing," Proc. SPIE 11822 (2021)
[16]. Vecchi, G., Salmaso, B., Basso, S., Sironi, G., et al., "BEaTriX, the Beam Expander Testing X-ray facility for testing ATHENA's SPO modules: the collimating mirror," Proc. SPIE 11119, 111191J (2019)
[17]. Christensen, F., Hornstrup, A., Frederiksen, P., et al., "Expanded beam x-ray optics calibration facility at the Daresbury Synchrotron," Proc. SPIE 2011, 540 (1994)
[18]. Sanchez del Rio, M., Cerrina, F., "Asymmetrically cut crystals for synchrotron radiation monochromators", Review of Scientific Instruments 63, 936 (1992)
[19]. Spiga, D., Salmaso, B., Bavdaz, M., Pelliciari, C., Basso, S., Burwitz, V., Ferreira, I., Ghigo, M., Giro, E., Pareschi, G., Sanchez del Rio, M., et al., "Optical simulations for the laboratory-based, expanded and collimated X-ray beam facility BEaTriX," Proc. SPIE 11110, 111100E (2019)
[20]. Ferrari, C., Beretta, S., Salmaso, B., Pareschi, G., Tagliaferri, G., et al., "Characterization of ADP crystals for soft x-ray optics of the Beam Expander Testing X-ray facility (BEaTriX)," Journal of Applied Crystallography 52, 599-604 (2019)
[21]. Vecchi, G., Cotroneo, V., Ghigo, M., Basso, S., Salmaso, B., Sironi, G., Spiga, D., Conconi, P., Pareschi, G., Tagliaferri, G., Burwitz, V., Hartner, G., Müller, T., Rukdee, S., Schmidt, T., Christensen, F., Della Monica Ferreira, D., Gellert, N., Massahi, S., Bavdaz, M., Ferreira, I., "Manufacturing and testing of the X-ray collimating mirror for the BEaTriX facility", Proc. SPIE 11822 (2021)
[22]. Sironi, G., Citterio, O., Pareschi, G., Negri, B., Ritucci, A., Subranni, R., Orlandi, A., Borghi, G., Stroebel, M., Arnold, J., Widemann, R., et al., "MPR: innovative 3D free-form optics profilometer," Proc. SPIE 8147, 814718 (2011)
[23]. Spiga, D., Raimondi, L., "X-ray optical systems: from metrology to Point Spread Function," Proc. SPIE 9209, 92090E (2014)
[24]. Spiga, D., Della Monica Ferreira, D., Shortt, B., Bavdaz, M., Bergback Knudsen, E., Bianucci, G., Christensen, F., Civitani, M., Collon, M., Conconi, P., Fransen, S., et al., "Optical simulations for design, alignment, and performance prediction of silicon pore optics for the ATHENA x-ray telescope," Proc. SPIE 10399, 103990H (2017)
[25]. Spiga, D., Moretti, A., Pareschi, G., Sironi, G., Tagliaferri, G., Bavdaz, M., Ferreira, I., Valsecchi, G., Marioni, F., Zocchi, F., "Optical simulations for the Wolter-I collimator in the VERT-X calibration facility," Proc. SPIE 11822 (2021)
[26]. B. Menz, H. Brauninger, V. Burwitz et al., "Studying ATHENA optics with divergent and collimated x-ray beams," Proc. SPIE 9144, 91445J (2014)